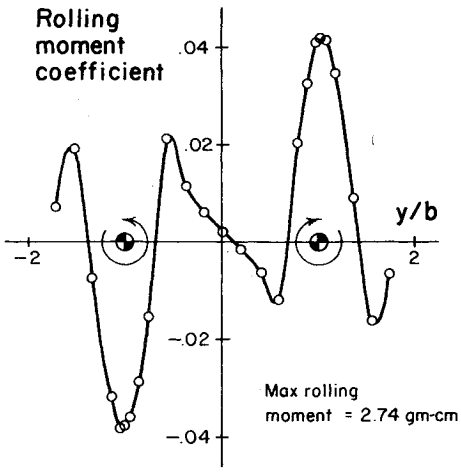

Fig. 4 Example of rolling moment data obtained with torque meter and model wing. The wing was traversed through a pair of counter-rotating line vortices located at $y/b = \pm 1$, where y is the lateral distance and b is the span of the model wing.

potentiometer. The output was measured on a digital dc voltmeter on the ±0.1 V full-scale range. The meter resolution was 0.01 mV.

The instrument was calibrated by hanging weights on the ends of the model wing. The calibration was found to be linear within about 1% throughout the ±5-deg range of allowable deflection. The value of the calibration factor was 3.85 mV/gm-cm (277 mV/oz-in.). Thus, the maximum expected rolling moment of 10 gm-cm (0.14 oz-in.) would produce a response of 38.5 mV with an angular deflection of only 0.76 deg. These characteristics were considered quite satisfactory. In fact, when the rolling moment measurements were made, the maximum values were found to be less than 3 gm-cm (0.04 oz-in.), so that the resulting angular deflections were in the neighborhood of 0.2 deg. For a voltmeter resolution of 0.01 mV, the torsional resolution of the torque meter is about 0.0003 gm-cm (3.6×10^{-6} oz-in.), with an angular resolution of 2×10^{-4} deg or 0.7 sec of arc. Of course, the latter figure is attributable to the RVDT itself and only depends on the torque meter design insofar as the alignment of its stator and rotor are concerned. If the more sensitive flexural pivots of the same size were to be used—with a combined sensitivity of 1.6 gm-cm/deg—the foregoing resolutions could be improved by a factor of 8.2.

One aspect of the design which could have proved troublesome is the lack of self-contained means of damping unwanted oscillations. For the rolling moment measurements, however, it was found that the aerodynamic damping of the wing model itself effectively reduced the amplitude of oscillations to an acceptable level. In anticipation of such a problem, the torque meter rotor was made as massive as possible to keep its undamped natural frequency as low as possible. This frequency turned out to be about 16 Hz, and it was a simple matter to make the time constant of the demodulation circuit short enough so that frequencies in this range had no measurable effect on the dc output. Viscous or eddy current damping devices could be added if necessary, however, and a space at the aft end of the instrument was provided for that purpose.

To illustrate the performance of the torque meter in the measurement of rolling moment, some typical data are shown in Fig. 4. The data show rolling moment coefficient of the wing model as it is traversed laterally through the center lines of a pair of counter-rotating parallel line vortices. The vortices are spaced apart a distance equal to twice the span of the model wing. They represent the adjacent tip vortices from two aircraft flying side by side so that a region of strong upwash is produced between them. The data are taken from Ref. 1. The torque meter proved to be extremely reliable and simple to use, and the resulting data were both repeatable and consistent with expected trends.

Although nominally designed for use in measuring torque, the instrument can be used, through modification of the wing mounting system, to measure the wing lift curve. To accomplish this, a crossarm is mounted at the end of the sting. The wing is fixed at one end of the arm with a means for adjusting angle of attack, and a counterweight is mounted at the other end. This arrangement was quite useful, although the aerodynamic damping of oscillations was not very effective as the wing approached stall.

Another possible use for this device would be as a nonrotating vorticity meter. For such an application, the instrument would function in the same way as it does when measuring rolling moment. For improved spatial resolution, however, the wing would be replaced by flat vanes of a size small enough to resolve vorticity gradients in the flow. The possibility of making a practical vorticity meter using this basic design is being investigated.

Acknowledgment

This work was sponsored by the Naval Air Development Center, Warminister, Pa., Contract N 62269-76-C-0305.

Reference

[1] Donaldson, C. duP., Bilanin, A. J., Williamson, G. G., and Snedeker, R. S., "Study of Feasibility of Conducting a Wake-Riding Experiment Using a T-2 Aircraft behind Two P-3 Aircraft," Aeronautical Research Associates of Princeton, Inc., Princeton, N.J., Rept. No. 287, Aug. 1976.

Aerodynamic Stability of Tethered Bodies

G. N. V. Rao*
Indian Institute of Science, Bangalore, India

Nomenclature

$OXYZ$	= fixed or inertial coordinate system
$O'X'Y'Z'$	= fixed body or moving coordinate system
X, Y, Z	= coordinates of a point with respect to $OXYZ$
s	= running distance along the cable measured from 0
σ	= complex frequency of Laplace transformation
ρ	= density of air
ρ_c	= mass per unit length of the cable
γ	= angle between an element of the cable and OYZ plane such that $\cos^2\gamma = (Y^2_s + Z^2_s)$
Subscripts	
o	= the equilibrium configuration
o'	= the property at O' with respect to O
s	= differentiation with respect to s
c	= the condition at the confluence point C in Fig. 1 and is placed before other subscripts

The rest of the symbols are standard and essentially the same as those in Ref. 1.

Received June 28, 1976; revision received Sept. 27, 1976.
Index categories: Aircraft Handling, Stability, and Control; Aircraft Performance.

*Associate Professor, Department of Aeronautical Engineering. Member AIAA.

Introduction

THE dynamic stability of tethered bodies such as balloons and airborne sensors has attracted considerable attention in recent times. A major improvement over the earlier studies[2,4-6] was made by DeLaurier[3] who included the cable dynamics, also. After linearization and other simplifications, DeLaurier reduced the cable equations to a set of wave equations with constant coefficients, and developed solutions which require a search for eigenvalues from a set of transcendental equations. A study of some of the cases revealed that when the body is being 'hauled in,' the tendency for instability is greater and that at short cable lengths, the variation of cable tension during oscillations (apparently not considered by DeLaurier) is significant and must be included. These considerations led to a reformulation of the problem to achieve three aims – 1) inclusion of variable tension during oscillations, 2) avoiding the complexity of search for eigenvalues in a set of transcendental equations, and 3) reducing the problem to a search for eigenvalues in a characteristic determinant with simple algebraic functions for the elements so that readily available computer based methods can be used. In the present study, these aims have been met after certain modifications were made which enable use of finite difference formulation.

Analysis

As an example, the dynamic stability of a tethered dirigible (Fig. 1) in a uniform wind U_0 along OX will be considered. Neglecting the virtual mass effect of the acceleration of the cable, the nonlinear cable equations along OX, OY, and OZ are

$$\rho_c \ddot{X} = (TX_s)_s + 1.1\ qd\cos^3\gamma \tag{1}$$

$$\rho_c \ddot{Y} = (TY_s)_s - (1.1\ qd\cos\gamma)(X_s Y_s) \tag{2}$$

$$\rho_c \ddot{Z} = (TZ_s)_s - (1.1\ qd\cos\gamma)(X_s Z_s) - \rho_c g \tag{3}$$

where T is the instantaneous cable tension, q is the instantaneous dynamic pressure equal to $[(U+\dot{X})^2 + \dot{Y}^2 + \dot{Z}^2][\rho/2]$, d is the diameter of the cable, and g is the acceleration due to gravity. $1.1\ qd\cos^2\gamma$ is the aerodynamic normal force on an element of the cable in the plane perpendicular to the OYZ plane and containing the element. Writing $X = X_0 + x$, $Y = Y_0 + y, \ldots$, $T = T_0 + \tau$, substituting in the cable equations, and neglecting terms of higher order than the first in the lower case letters, one can obtain the linearized perturbation equations with variable coefficients. If it is assumed that the equilibrium configuration of the cable lies in the XOZ plane, such that $Y_{os} = Y_{oss} = 0$, the following Laplace transformed equations are obtained, where the lower case letters now represent the transformed variables.

$$(\rho_c\sigma^2 + M_1\sigma)x = (T_0 x_s)_s + (\tau X_{os})_s + M_2 x_s + M_3 z_s \tag{4}$$

$$\rho_c\sigma^2 y = (T_0 y_s)_s - 0.55\ \rho U^2{}_o d X_{os} Z_{os} y_s \tag{5}$$

$$\rho_c\sigma^2 z + M_4\sigma x = (T_0 z_s)_s + (\tau Z_{os})_s + M_5 x_s + M_6 z_s \tag{6}$$

In the preceding equations, $M_1, M_2, \ldots, M_6$ are functions of s, obtained from the equilibrium configuration. The direction cosines of the cable element satisfy the following relations in the equilibrium and perturbed states.

$$X^2{}_{os} + Z^2{}_{os} = 1 \tag{7}$$

$$X_{os}X_{oss} + Z_{os}Z_{oss} = 0 \tag{8}$$

$$X_{os}x_s + Z_{os}z_s = 0 \tag{9}$$

$$X_{os}x_{ss} + Z_{os}z_{ss} + X_{oss}x_s + Z_{oss}z_s = 0 \tag{10}$$

The uncoupling of the longitudinal and lateral motions may be noted. Multiplying Eqs. (4 and 6) by X_{os} and Z_{os}, respectively, adding and using Eqs. (7-9), one obtains

$$\tau_s = a_{11}x_{ss} + a_{12}z_{ss} + a_{13}x_s + a_{14}z_s + a_{15}x + a_{16}z \tag{11}$$

A similar operation with X_{oss} and Z_{oss} yields

$$\tau = b_{11}x_{ss} + b_{12}z_{ss} + b_{13}x_s + b_{14}z_s + b_{15}x + b_{16}z \tag{12}$$

One can now eliminate z_{ss} in Eqs. (11 and 12) by using Eq. (10), and also express z_s in terms of x_s from Eq. (9). When these substitutions are made, one obtains

$$\tau_s = c_{11}x_s + c_{12}x + c_{13}z \tag{13}$$

$$\tau = d_{11}x_{ss} + d_{12}x_s + d_{13}x + d_{14}z \tag{14}$$

On differentiating Eq. (14) with respect to s and equating to Eq. (13), a third-order differential equation of the type given below will be obtained.

$$g_{11}x_{sss} + g_{12}x_{ss} + g_{13}x_s + g_{14}x + g_{15}z = 0 \tag{15}$$

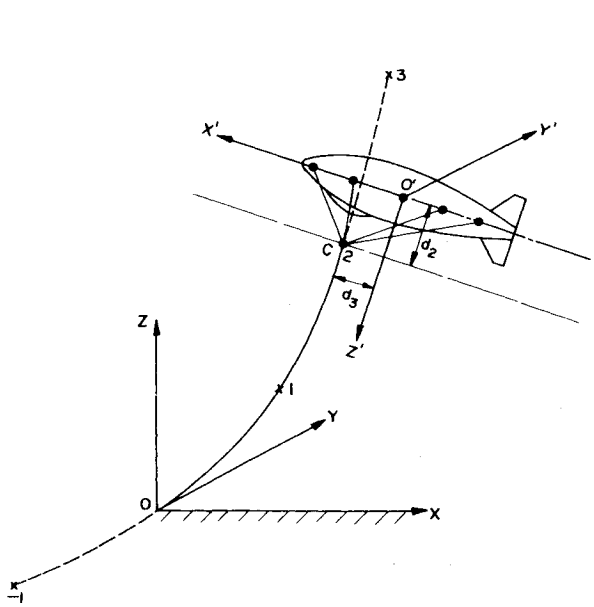

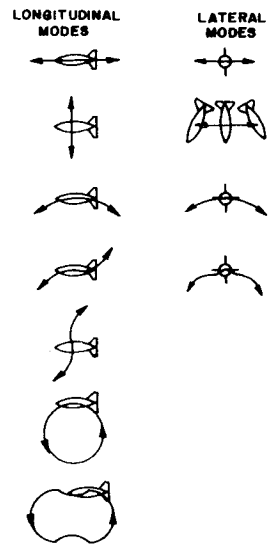

Fig. 1 Geometry of tethered kytoon.

Equations (5 and 15) may be viewed as the two cable equations. The coefficients in both these equations depend on the equilibrium configuration and in some cases also on the complex frequency σ. For example

$$g_{15}=\frac{\rho_c\sigma^2 Z_{osss}}{\Delta_o}-\frac{2\rho_c\sigma^2 Z_{oss}\,(X_{oss}X_{osss}+Z_{oss}Z_{osss})}{\Delta_o^2} \tag{16}$$

where

$$\Delta_o=(X^2{}_{oss}+Z^2{}_{oss}) \tag{17}$$

The boundary conditions at $s=0$, are, $x=0$, $y=0$, and $z=0$. At $s=L$, where L is the length of the cable, the displacement of the confluence point C (Fig. 1) from equilibrium as the end of the cable must be equal to the displacement of C as a part of the body. This requirement leads to the relations given later in Eqs. (25-27).

In order to deal only with variable x when considering longitudinal motion, one can use Eq. (9) which, when integrated for z gives,

$$z=-[(X_{os}/Z_{os})x-\int_o^s(\Delta_o x)/(Z_{os}X_{oss})\,ds] \tag{18}$$

In the scheme of computations suggested, a certain number of pivotal points are chosen on the cable and beyond it, and the equilibrium properties at these points evaluated. Let the perturbation variables at these pivotal points be designated by x_i, y_i, and z_i. Then the integral in Eq. (18) can be replaced by a sum and z_i expressed in terms of x_i. This applies also to the boundary values x_{cs}, y_{cs}, and z_{cs}. The equilibrium properties at these pivotal points enable one to transform Eqs. (5 and 15) into a set of finite difference equations using Eq. (18) in Eq. (15).

The preceding equations have to be supplemented by the equations of motion of the body. These equations are, in the usual notations

$$(X'_u-\sigma m)u+X'_w w-(B_f-mg)\theta\cos\theta_o-(X_{\cos}\cos\theta_o-Z_{\cos}\sin\theta_o)\tau+(T_{co}X_{\cos}\sin\theta_o+T_{co}Z_{\cos}\cos\theta_o)\theta-x_{cs}T_{co}\cos\theta_o+z_{cs}T_{co}\sin\theta_o=0 \tag{19}$$

$$(Y'_v-\sigma m)v-(mU_o^2\cos\theta_o+Y'_p\sin\theta_o-Y'_r\cos\theta_o-T_{co}X_{\cos})\psi+[Y'_p\sigma+(mg-B_f)\cos\theta_o-T_{co}X_{\cos}\sin\theta_o-T_{co}Z_{\cos}\cos\theta_o]\phi-y_{cs}T_{co}=0 \tag{20}$$

$$Z'_u u+(Z'_w-\sigma m+\sigma Z'_w)w+[Z'_q\sigma+m\cos\theta_o+(mg-B_f)\sin\theta_o-T_{co}X_{\cos}\cos\theta_o+T_{co}Z_{\cos}\sin\theta_o]0-(X_{\cos}\sin\theta_o+Z_{\cos}\cos\theta_o)\tau-x_{cs}T_{cs}\sin\theta_o-z_{cs}T_{co}\cos\theta_o=0 \tag{21}$$

$$L_v v-(A\sigma^2-L_p\sigma+d_2T_{co}X_{\cos}\sin\theta_o+d_2T_{co}Z_{\cos}\theta_o)\phi+(A\sigma^2\sin\theta_p+E\sigma^2\cos\theta_0-L_p\sigma\sin\theta_o+L_r\sigma\cos\theta_o)\psi+d_2T_{co}y_{cs}=0 \tag{22}$$

$$M_u u+(M_w+\sigma M_w)w+[M_q\sigma-B\sigma^2+d_3(T_{co}X_{\cos}\sin\theta_o-B_f\sin\theta_o+T_{co}Z_{\cos}\cos\theta_o)-d_2(T_{co}X_{\cos}\cos\theta_o-T_{co}Z_{\cos}\sin\theta_o)]\theta-[d_3(X_{\cos}\cos\theta_o-Z_{\cos}\sin\theta_o)+d_2(X_{\cos}\sin\theta_o+Z_{\cos}\cos\theta_o)]\tau-x_{cs}(d_3T_{co}\cos\theta_o+d_2T_{co}\sin\theta_o)+z_{cs}(d_3T_{co}\sin\theta_o-d_2T_{co}\cos\theta_o)=0 \tag{23}$$

$$N_v v-(C\sigma^2\cos\theta_o+E\sigma^2\sin\theta_o+N_p\sigma\sin\theta_o-N_r\sigma\cos\theta_o+d_3T_{co}X_{\cos})\psi+[E\sigma^2+N_p\sigma+d_3X_{\cos}T_{co}\sin\theta_o+d_3Z_{\cos}T_{co}\cos\theta_o]\phi+d_3T_{co}y_{cs}=0 \tag{24}$$

The displacement of the point C as a part of the body is given by the following trajectory equations.

$$X_c=(1/\sigma)u\cos\theta_o+(1/\sigma)w\sin\theta_o-\theta[d_3\sin\theta_o-d_2\cos\theta_o+(1/\sigma)U_o\sin\theta_o\cos\theta_o] \tag{25}$$

$$Y_c=(1/\sigma)v+[(1/\sigma)(U_0\cos^2\theta_o)+d_3\cos\theta_o+d_2\sin\theta_o]\psi-d_2\phi \tag{26}$$

$$Z_c=-(1/\sigma)u\sin\theta_o+(1/\sigma)w\cos\theta_o-[d_3\cos\theta_o+d_2\sin\theta_o-(1/\sigma)U_o\cos\theta_o]\theta \tag{27}$$

Eqs. (15, 19, 21, 23, 25, and 27) constitute the longitudinal set and they are uncoupled from the lateral set of Eqs. (5, 20, 22, 24, and 26). We seek solutions of the preceding equations in terms of function values at a certain number of points. An example is briefly illustrated by considering five pivotal points on the cable as shown in Fig. 1 at $s=-(L/2)$, $s=0$, $s=(L/2)$, $s=L$, and $s=1.5\ (L/2)$. The characteristic equation for the longitudinal motion is then found to be of the form

$$a_1\sigma^{14}+a_2\sigma^{13}+a_3\sigma^{12}\ldots+a_{15}=0 \tag{28}$$

The corresponding oscillatory modes are eight in number and consist of three "pure" modes (longitudinal, vertical, and pitching), three coupled among two of the three variables, (longitudinal with pitching, vertical with pitching, and pitching with longitudinal) and combined pitching, longitudinal and vertical. These are sketched in Fig. 1.

A similar analysis with the lateral motion equations yield

$$b_1\sigma^9+b_2\sigma^8+b_3\sigma^7\ldots+b_{10}=0 \tag{29}$$

This consists of four oscillatory modes, 1) lateral oscillations with no yaw, 2) lateral oscillation with yaw, 3) rolling of the body with insignificant motion of the cable, and 4) combined lateral, yawing, and rolling motions, together with a roll convergence case. These are also sketched in Fig. 1. In practice, there is no difficulty in increasing the number of pivotal points except the limitation imposed by the memory of the computer and the possible need to use double precision in dealing with large determinants.

References

[1] Etkin, B., *Dynamics of Flight*, Wiley, N.Y., 1959.

[2] Etkin, B. and Mackworth, J. C., "Aerodynamic Instability of Non-Lifting Bodies Towed Beneath an Aircraft," University of Toronto, UTIA TN 65, 1963.

[3] DeLaurier, J. D., "A Stability Analysis for Tethered Aerodynamically Shaped Balloons," *Journal of Aircraft*, Vol. 9, Sept. 1972, pp. 646-651.

[4] Glauert, H., "The Stability of a Body Towed by a Light Wire," Aeronautical Research Council, London, R&M 1312, 1930.

[5] Neumark, S., "Equilibrium Configurations of Flying Cables of Captive Balloons and Cable Derivatives for Stability Calculations," Aeronautical Research Council, London, R&M 3333, 1963.

[6] Redd, T. L., Bland, S. R., and Bennett, R. M., "Stability Analysis and Trend Study of a Balloon Tethered in a Wind with Experimental Comparisons," NASA TN D-7272, Oct. 1973.